Atomic-Scale Insights into the Interlayer Characteristics and Oxygen Reactivity of Bilayer Borophene

Linfei Li,^[a] Jeremy F. Schultz,^[a] Sayantan Mahapatra,^[a] Xiaolong Liu,^[b] Xu Zhang,^[c] Mark C. Hersam,^[d,e,f] and Nan Jiang*^[a]

- [a] Dr. L. Li, Dr. J. F. Schultz, Dr. S. Mahapatra, Prof. N. Jiang Department of Chemistry, University of Illinois Chicago Chicago, Illinois 60607, United States
- E-mail: njiang@uic.edu
- [b] Prof. X. Liu Department of Physics and Astronomy, University of Notre Dame Notre Dame, Indiana 46556, United States
- Prof. X. Zhang
 Department of Physics and Astronomy, California State University
 Northridge, California 91330-8268, United States
- Prof. M. C. Hersam
 Department of Materials Science and Engineering, Northwestern University
 Evanston, Illinois 60208-3108, United States
- [e] Prof. M. C. Hersam
 Department of Chemistry, Northwestern University
 Evanston, Illinois 60208-3108, United States
- [f] Prof. M. C. Hersam
 Department of Electrical and Computer Engineering, Northwestern University
 Evanston, Illinois 60208-3108, United States

Abstract: Bilayer (BL) two-dimensional boron (i.e., borophene) has recently been synthesized and computationally predicted to have promising physical properties for a variety of electronic and energy technologies. However, the fundamental chemical properties of BL borophene that form the foundation of practical applications remain unexplored. Here, we present atomic-level chemical characterization of BL borophene using ultrahigh vacuum tip-enhanced Raman spectroscopy (UHV-TERS). UHV-TERS identifies the vibrational fingerprint of BL borophene with angstrom-scale spatial resolution. The observed Raman spectra are directly correlated with the vibrations of interlayer boron-boron bonds, validating the threedimensional lattice geometry of BL borophene. By virtue of the single-bond sensitivity of UHV-TERS to oxygen adatoms, we demonstrate the enhanced chemical stability of BL borophene compared to its monolayer counterpart by exposure to controlled oxidizing atmospheres in UHV. In addition to providing fundamental chemical insight into BL borophene, this work establishes UHV-TERS as a powerful tool to probe interlayer bonding and surface reactivity of low-dimensional materials at the atomic scale.

Introduction

Recently, bilayer (BL) and few-layer graphene and transition metal dichalcogenides in well-controlled stacking geometries have attracted immense interest due to their exotic and finely tunable physical properties.^[1] Unlike these natural layered materials that can be exfoliated and integrated mechanically due to interlayer van der Waals (vdW) interactions,^[2] synthetic two-dimensional (2D) materials have no bulk counterparts^[3] and thus form layered structures potentially via non-vdW interactions. Very recently, the first BL synthetic 2D boron (i.e., borophenel^[4]) was realized on Ag(111) substrates^[5] with enhanced stability^[6] and promising computationally predicted properties such as superconductivity,^[7] antiferromagnetism,^[8] double Dirac cones,^[9] and nodal line fermions.^[10] In contrast to vdW-coupled bilayer 2D

materials, BL borophene features two borophene monolayers covalently linked by interlayer boron-boron (B-B) bonds. In addition to its structural characteristics, insights into the chemistry of BL borophene, especially the nature of interfacial interactions and surface reactivity, are crucial to tailoring its intriguing properties and realizing its full potential for practical applications. However, the chemistry of BL borophene on Ag(111) remains unexplored due to several challenges. First, BL borophene domains grown on Ag(111) are typically dozens of nanometers in size and surrounded by polymorphic single-layer (SL) borophene (thus forming mixed-dimensional borophene),^[5] which necessitates characterization with nanoscale chemical spatial resolution. Second, while the interlayer bonding characteristics of BL borophene play a key role in its chemical stability and fundamental properties, [5, 11] these interlayer bonds are physically buried and thus cannot be directly interrogated via common surface imaging techniques, such as scanning probe microscopy (SPM), due to their limited subsurface resolution and minimal chemical sensitivity.

By combining Raman spectroscopy with ultrahigh vacuum (UHV) scanning tunneling microscopy (STM), UHV tip-enhanced Raman spectroscopy (UHV-TERS) has been recently developed to investigate chemistry at the ultimate spatial limit. [12] With angstrom-scale resolution, UHV-TERS is a powerful tool to interrogate site-specific chemical properties of 2D materials and interlayer interactions of layered structures. [13] For example, UHV-TERS has been employed to characterize atomic-level lattice strains and oxidative behaviors of borophene monolayers. [14]

In this study, we use combined UHV-TERS, UHV-STM, and density functional theory (DFT) calculations to probe the interlayer characteristics and chemical stability of BL borophene on Ag(111) at the atomic scale. We establish that the Raman spectra of BL borophene can be directly correlated with the vibrations of interlayer B-B bonds, which allows BL borophene to be identified and imaged chemically with angstrom-scale spatial resolution. To explore its chemical stability, we expose

BL borophene to controlled oxidizing atmospheres in UHV. In contrast to highly reactive SL borophene, BL borophene shows significantly enhanced inertness to oxidation, as evidenced by atomic-resolution STM imaging and TERS measurements. The observed oxidation resistance and structural integrity of BL borophene are corroborated by DFT calculations. Overall, this work establishes atomic-level insights into the fundamental structural and chemical properties of BL borophene, paving the way for future utilization of BL borophene in practical applications.

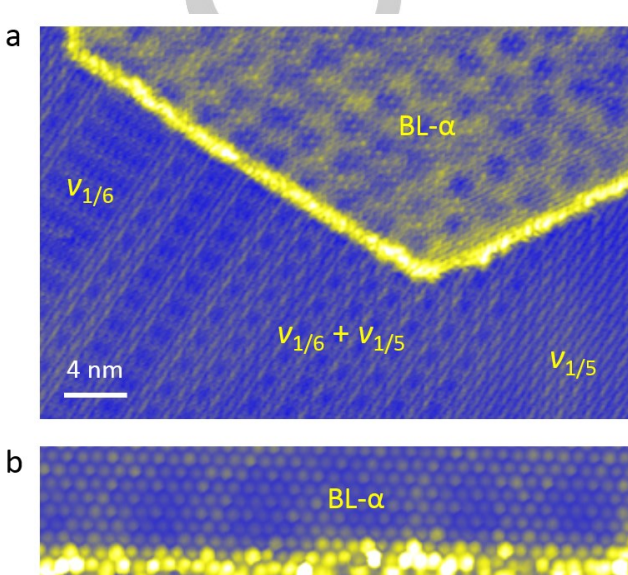
Results and Discussion

BL borophene was prepared by nucleation and growth after evaporating boron onto Ag(111) surfaces beyond full monolayer coverage (see Methods in the Supporting Information).^[5] It was found that BL borophene growth is favored at relatively low temperatures, below 450 $^{\circ}\text{C}$ (in contrast to < 550 $^{\circ}\text{C}$ for SL borophene growth), where SL borophene exists in the form of pure $v_{1/6}$ phase or mixed phase $(v_{1/6} + v_{1/5})$.[14b, 15] Consequently, BL borophene is typically surrounded by SL borophene polymorphs (Figure 1a), resulting in mixed-dimensional borophene with the lattice of BL borophene extending in the third dimension. The incommensurate lattices between SL and BL borophene give rise to phase boundaries with high local density of states, as highly resolved in Figure 1b. These electronically active interfaces suggest preferential sites to host adsorbates (e.g., oxygen). Figure 1c shows the atomic structures of the $v_{1/6}$, $v_{1/5}$, and BL- α borophene phases. A SL borophene lattice is constructed by periodically arranged hexagonal vacancies with various concentrations (vn: n denotes the concentration of hexagonal vacancies in an otherwise triangular lattice). [4, 14b, 15] In particular, BL-α borophene has been postulated to consist of two identical $v_{1/9}$ borophene monolayers in an AA stacking geometry that are covalently coupled via interlayer B-B bonds. [5-6]

Although the BL $v_{1/9}$ lattice matches atomic-resolution SPM images, ^[5] this prior characterization cannot fully rule out other possible BL borophene lattice motifs, given that SPM images reflect the convolution of topographic and electronic information or tip-sample atomic forces. In particular, SPM characterization of bilayer structures is challenging due to the low sensitivity of SPM to subsurface lattices and interlayer bonding. Alternatively, due to its direct measurement of the vibrational behavior of chemical bonds, TERS can identify atomic structures based on their vibrational signatures. The combined ability of TERS to capture both topographic and vibrational information at the subnanometer scale is especially beneficial for interlayer feature characterization and surface chemical imaging, thus allowing unambiguous identification and comprehensive understanding of layered structures.

In this context, we performed TERS studies of mixed-dimensional borophene polymorphs. As shown in Figure 2b, distinct Raman spectral profiles are acquired when the TERS tip is placed on the Ag(111), SL, and BL borophene surfaces shown in Figure 2a. In contrast to the featureless spectrum (black) collected on Ag(111), a 189 cm⁻¹ peak dominates the spectrum (green) acquired on SL borophene, which is readily assigned to the characteristic Raman mode of SL $v_{1/6}$ borophene as demonstrated previously (Figure 2b bottom model). [14b] Notably, a new peak located at 317 cm⁻¹ is observed on the BL

borophene island as marked by a red plus. The observed 317 cm⁻¹ Raman mode is in close agreement with DFT simulations based on a BL $v_{1/9}$ borophene structure (318 cm⁻¹ simulated), as shown schematically in Figure 2b (top model, more views shown in Figure S1). Specifically, this Raman mode is dominated by the vertical vibrations of interlayer B–B bonds, thereby confirming the interlayer covalently bonded nature of BL borophene. The absence of the 189 cm⁻¹ mode in the TERS spectrum of BL borophene phase indicates the discontinuity of $v_{1/6}$ borophene monolayers across the BL borophene island. In other words, BL borophene is chemically distinct from the surrounding SL $v_{1/6}$ borophene nor composed of $v_{1/6}$ borophene sublayers.



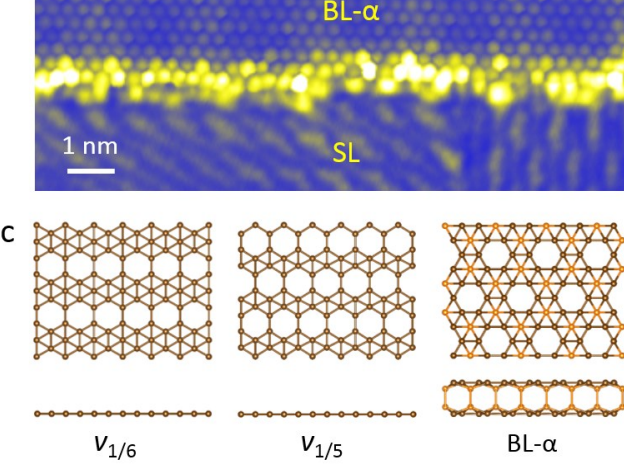


Figure 1. Growth and atomic structure of BL borophene on Ag(111). a) Constant-current STM topography of a BL borophene island surrounded by SL borophene polymorphs. b) Constant-height STM image of the interface between SL and BL borophene acquired with a CO-functionalized tip. c) Schematic of SL $v_{1/6}$, SL $v_{1/6}$, and BL-α borophene structures in plan view (top) and cross-sectional view (bottom). Orange balls and sticks represent inward-buckled boron atoms and corresponding interlayer B–B bonds, respectively. Tunneling conditions: (a) 32 mV, 610 pA; (b) 20 mV, 69 pA.

TERS spatial mapping provides further chemical differentiation of BL and SL borophene. As shown in Figure 2c, by collecting 64 sequential TERS spectra over a mixed-phase borophene surface (marked with a box in Figure 2a) and then tracking the intensity of the 317 cm⁻¹ band, we acquired a TERS

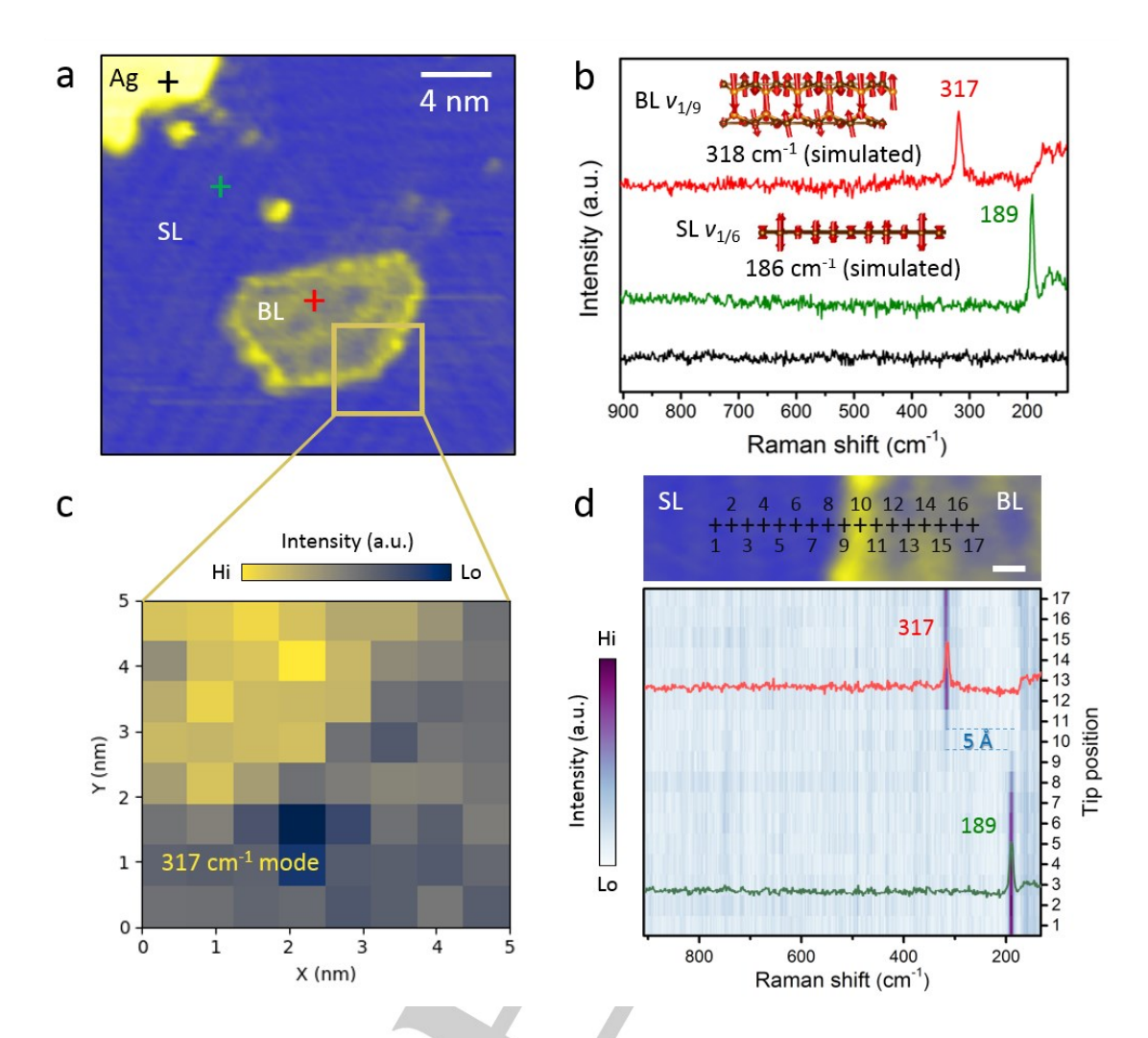


Figure 2. Chemical fingerprinting and imaging of BL borophene with UHV-TERS, a) STM image of SL and BL borophene grown on Ag(111). b) TERS spectra acquired on the sites marked with pluses in (a). Inset: side views of the atomic displacements of simulated Raman modes in SL and BL borophene (more views shown in Figure S1 for clarity). c) TERS intensity mapping of the 317 cm⁻¹ Raman mode over the area indicated in (a). d) TERS line scan along the trace in the STM image across the interface between SL $v_{1/6}$ borophene and BL borophene. Two representative Raman spectra are superimposed. Scale bar: 1 nm. Tunneling conditions: (a,d) 1.3 V, 100 pA. TERS parameters: (b) 200 mV, 1 nA, 10 s acquisition time; (c) 100 mV, 1 nA, 3 s per pixel; (d) 200 mV, 1 nA, 5 s per point with a step length of 5 Å.

map where the BL borophene phase located in the top left corner of the scanned area is chemically imaged. To probe the spectral evolution across the interface between BL and SL borophene, we performed a TERS line scan along the trace indicated in the STM image in Figure 2d with a step length of 5 Å. In addition to reproducing the characteristic 189 and 317 cm⁻¹ modes of the SL $v_{1/6}$ and BL $v_{1/9}$ borophene, respectively, TERS measurements display low Raman intensities of borophene at the SL-BL boundary (i.e., around position 10) over a range of 5-10 Å. This localized suppression of both borophene vibrational modes suggests incommensurate interfacial lattices between SL and BL borophene, which results in structural disorder and dangling bonds as shown in Figure 1b and ultimately underlies a susceptibility to oxidation as discussed later. Similar TERS profile features were observed at the interface between SL $v_{1/5}$ and BL borophene (Figure S2), again revealing the distinctive chemical nature of BL borophene from that of SL borophene polymorphs.

SL borophene has been demonstrated to oxidize and degrade significantly upon exposure to oxygen or air (Figure S3), [4a, 14a] impeding further processing and device fabrication. In contrast to the planar network of SL borophene, the three-dimensional (3D) lattice of BL borophene allows for charge transfer and redistribution within BL borophene via interlayer B-B bonds, [5-6, 11] which likely influences chemical reactivity. Since no fundamental study of the chemical reactivity of BL borophene on Ag(111) had been conducted, we investigated the chemical stability and structural integrity of BL borophene in controlled oxidizing atmospheres in UHV.

Figure 3a shows an STM topographic derivative map of mixed-dimensional borophene following exposure to 300 L (1 L = 1 \times 10⁻⁶ torr s) of molecular oxygen at room temperature in UHV. SL borophene is observed to be dotted with uniform protrusions, whereas BL borophene remains unchanged. Given their distinct oxygen affinities, site-resolved chemical interrogation of oxidized mixed-dimensional borophene becomes

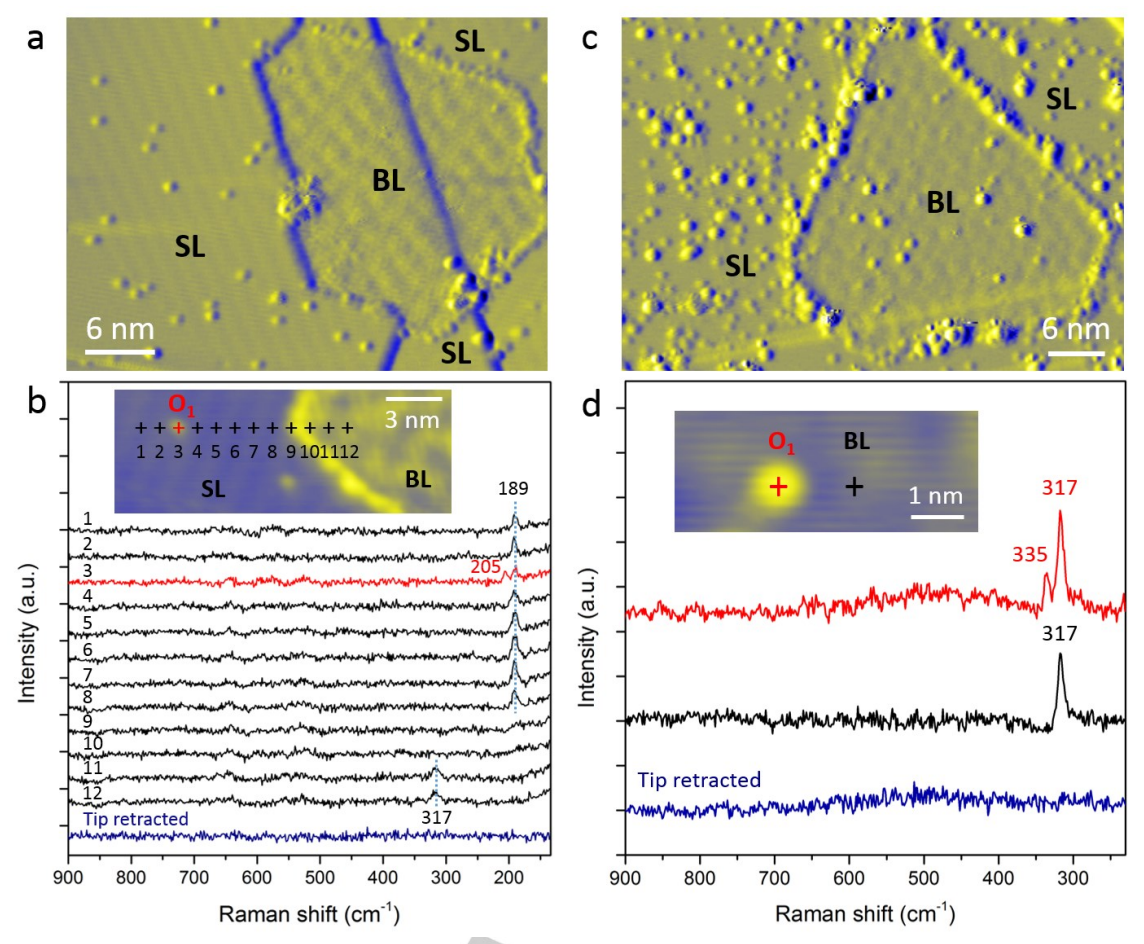


Figure 3. Atomic-scale chemical insights into the oxidation of mixed-dimensional borophene. a) Topographic derivative STM image of SL and BL borophene following exposure to a low dose of O_2 (300 L) in UHV. b) TERS line scan along the tip trace shown in the inset STM image across an oxygen adatom on SL borophene. c) Topographic derivative STM image of SL and BL borophene after exposure to a high dose (1800 L) of O_2 . d) TERS spectra on oxidized BL borophene shown in the inset STM image. Tunneling conditions: (a) 1.0 V, 55 pA; (b) 1.2 V, 100 pA; (c) 0.7 V, 60 pA; (d) 0.7 V, 300 pA. TERS parameters: (b) 100 mV, 1 nA, 5 s per point with a step length of 1 nm; (d) 200 mV, 1 nA, 30 s.

necessary to identify the oxidation properties of SL and BL 3b borophene. Figure shows 12 sequential measurements along the tip trace shown in the inset STM image, which is across a protrusion on the SL borophene and the SL-BL borophene boundary. The exceptional spatial resolution of TERS enables the identification of two Raman modes at 205 and 189 cm⁻¹ for the protrusion (position 3) that have previously been assigned to the vibrational fingerprint of single oxygen adatoms on SL $v_{1/6}$ borophene.^[14a] The dissociative adsorption of oxygen on SL borophene underlies its oxygen reactivity at room temperature.[14a, 16] In contrast to O-modified SL borophene surfaces, the basal plane of BL borophene remains chemically intact, showing the characteristic 317 cm⁻¹ mode of pristine BL borophene (positions 11 and 12). The featureless Raman profiles acquired at BL borophene edges (positions 9 and 10) suggest that BL borophene edges have not been significantly modified following this low O₂ exposure.

The topographic evolution of SL and BL borophene with increasing oxygen exposure is shown in Figure S4. In particular, BL borophene edges are increasingly degraded with disordered clusters upon exposure to a high dose of O_2 (1800 L) (Figure 3c).

The high oxygen affinity of the BL borophene edges can be attributed to under-coordinated boron, as demonstrated by theoretical simulations (Figure S5). With distinctive Raman features, these edge clusters could be ascribed to boron oxide species of high diversity (Figure S6), as found at the oxidized edges of SL borophene. [144a, 16] At these high oxygen dosing conditions, SL borophene is heavily modified with inhomogeneous particles. In contrast, the terrace of the BL borophene island remains relatively inert to oxidation, even in a harsher condition with exposure to atomic oxygen (Figure S7).

Despite its high chemical inertness, the basal plane of BL borophene is slightly modified following high O_2 doses. Specifically, STM revealed a few protrusions on BL borophene (Figure 3c). We tentatively assigned these protrusions to oxygen adatoms, as they are qualitatively similar to atomic oxygen adsorbed on SL borophene (Figure 3a). TERS was then used to determine the chemical nature of these atomic-scale adsorbates. As shown in Figure 3d, two Raman peaks located at 317 and 335 cm⁻¹ are observed for a small protrusion on BL borophene, in contrast to the sole Raman band at 317 cm⁻¹ for pristine BL borophene.

RESEARCH ARTICLE WILEY-VCH

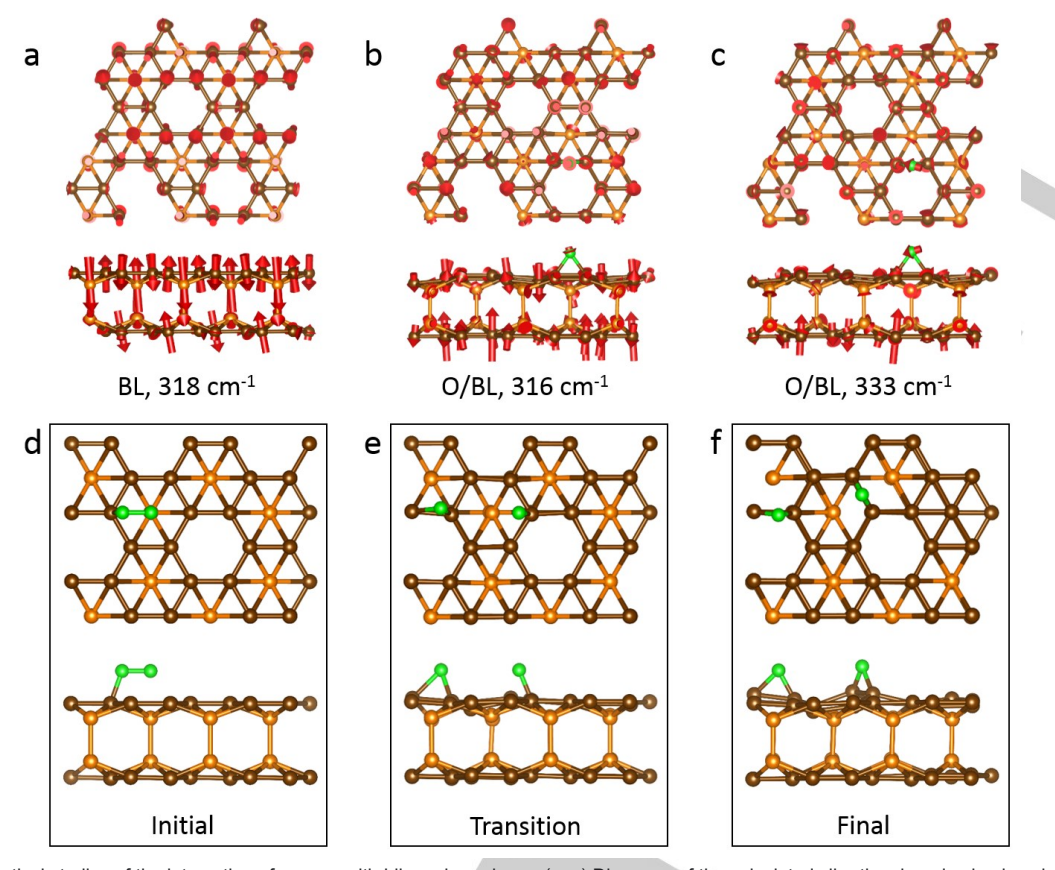


Figure 4. Theoretical studies of the interaction of oxygen with bilayer borophene. (a-c) Diagrams of the calculated vibrational modes in plan view (top) and cross-sectional view (bottom) corresponding to the experimental Raman bands shown in Fig. 3d. Green balls and sticks represent oxygen atoms and corresponding B-O bonds. Ag substrate atoms are not plotted for clarity. (d-f) Schematic illustration of the dissociation process of molecular oxygen (green) on BL borophene.

To interpret the observed spectral features, DFT simulations were carried out to determine the vibrational modes for an Obonded BL borophene configuration. Two vibrational frequencies at 316 and 333 cm⁻¹ were identified (Figure 4b,c), in excellent agreement with the experimental TERS peaks at 317 and 335 cm⁻¹, respectively. In particular, both Raman modes contain B–O vibrations. Note that the calculated 316 cm⁻¹ mode of O/BL borophene (Figure 4b) is very close in energy to the 318 cm⁻¹ mode of pristine BL borophene (Figure 4a). Given the spectral resolution of 4–5 cm⁻¹ for our TERS system, these two modes are apparently overlapped and thus observed experimentally at 317 cm⁻¹ in the O/BL borophene spectrum (Figure 3d, red spectrum).

Additional DFT calculations were performed to gain further chemical insight into the interaction between oxygen and BL borophene. As shown in Figure 4d-f, DFT simulations suggest that molecular oxygen is thermodynamically unstable during adsorption onto BL borophene resulting in spontaneous dissociation into atomic oxygen without energy barriers. This is in contrast to the dissociation process of molecular oxygen on SL borophene where an energy barrier of up to 0.39 eV is needed.[17] The dissociated oxygen atoms preferentially adsorb to the bridge sites of the BL borophene lattice that covalently link two adjacent boron atoms with an adsorption energy of 3.91 eV, which is higher than that on SL borophene (2.51 eV, Figure S8).[17b] These remarkable energy differences in oxygen reactivity could be attributed to charge redistribution within the BL borophene lattice that plays a key role in charge transfer between adsorbed oxygen species and borophene. Note that the higher adsorption energy of atomic oxygen on BL borophene suggests a stronger B-O bond on BL borophene, which apparently contradicts the observed low oxygen affinity of BL borophene.

To address this issue, we studied the dynamics of adsorbed oxygen, which could shed light on the oxidation resistance and structural integrity of BL borophene surfaces. Specifically, we investigated the migration of oxygen adatoms on BL borophene with the energy profile along an optimized diffusion pathway displayed in Figure S9. The diffusion barrier was calculated to be 0.67 eV, which is much smaller than that of atomic oxygen on SL borophene (0.88-1.37 eV)^[17a] and graphene (0.81 eV).^[18] Note that the real diffusion barrier could be further reduced due to the strong charge doping of BL borophene by metal substrates, a scenario that has been demonstrated in the case of oxygen diffusion on graphene.[19] Ultimately, this diffusion energy is sufficient for diffusion at room temperature. Consequently, oxygen atoms diffuse across BL borophene surfaces until they are chemisorbed at defect sites on the basal plane or at the edges of BL borophene islands. Since BL borophene has been demonstrated to have superior crystallinity,[5] atomic oxygen chemisorption is expected to occur predominately at the edges of BL borophene rather than on its highly crystalline surface, consistent with our experimental observations (Figure 3c and Figure S4) and theoretical calculations (Figure S5).

Conclusion

In summary, we have studied the interfacial characteristics and oxidative properties of BL borophene at the atomic scale using combined UHV-STM and UHV-TERS. In addition to atomicresolution imaging of the top layer lattice, STM-TERS provides vibrational information about interlayer bonds, thereby establishing the chemical fingerprint of the 3D lattice of BL borophene. In contrast to highly reactive borophene monolayers, BL borophene shows high oxidation resistance, a crucial characteristic needed for fundamental studies and technological applications. Given the increasing interest in borophene and the limited availability of air-stable borophene phases,[20] this work provides critical insight for harvesting the desirable properties of 2D boron structures through interlayer bonding in BL borophene. In addition, we demonstrate UHV-TERS as a powerful method to investigate chemically inhomogeneous surfaces and mixeddimensional structures on the atomic level, which can be generalized to studies of the structural characteristics and chemical properties of other multi-layer low-dimensional materials.

Acknowledgements

N.J. and L.L. acknowledge support from the National Science Foundation (DMR-2211474). X.Z. acknowledges support from the National Science Foundation (DMR-1828019). M.C.H. acknowledges support from the Office of Naval Research (ONR N00014-21-1-2679) and the National Science Foundation Materials Research Science and Engineering Center (NSF DMR-1720139).

Keywords: Borophene • interlayer interactions • scanning probe microscopy • tip-enhanced Raman spectroscopy • two-dimensional materials

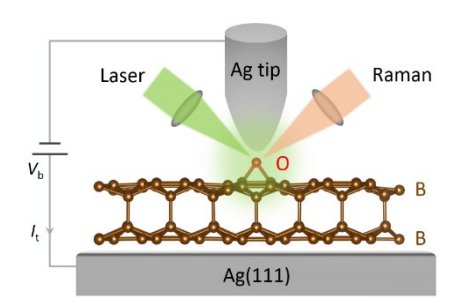
- a) Y. Cao, V. Fatemi, S. Fang, K. Watanabe, T. Taniguchi, E. Kaxiras, P. Jarillo-Herrero, Nature 2018, 556, 43-50; b) Y. Cao, V. Fatemi, A. Demir, S. Fang, S. L. Tomarken, J. Y. Luo, J. D. Sanchez-Yamagishi, K. Watanabe, T. Taniguchi, E. Kaxiras, R. C. Ashoori, P. Jarillo-Herrero, Nature 2018, 556, 80-84; c) E. Y. Andrei, A. H. MacDonald, Nat. Mater. 2020, 19, 1265-1275; d) D. M. Kennes, M. Claassen, L. D. Xian, A. Georges, A. J. Millis, J. Hone, C. R. Dean, D. N. Basov, A. N. Pasupathy, A. Rubio, Nat. Phys. 2021, 17, 155-163; e) G. R. Chen, A. L. Sharpe, P. Gallagher, I. T. Rosen, E. J. Fox, L. L. Jiang, B. S. Lyu, H. Y. Li, K. Watanabe, T. Taniguchi, J. Jung, Z. W. Shi, D. Goldhaber-Gordon, Y. B. Zhang, F. Wang, Nature 2019, 572, 215-219; f) E. C. Regan, D. Q. Wang, C. H. Jin, M. I. Utama, B. N. Gao, X. Wei, S. H. Zhao, W. Y. Zhao, Z. C. Zhang, K. Yumigeta, M. Blei, J. D. Carlstrom, K. Watanabe, T. Taniguchi, S. Tongay, M. Crommie, A. Zettl, F. Wang, Nature 2020, 579, 359-363; g) Y. H. Tang, L. Z. Li, T. X. Li, Y. Xu, S. Liu, K. Barmak, K. Watanabe, T. Taniguchi, A. H. MacDonald, J. Shan, K. F. Mak, Nature 2020, 579, 353-358.
- a) K. S. Novoselov, A. Mishchenko, A. Carvalho, A. H. C. Neto, Science 2016, 353, aac9439; b) Y. Liu, N. O. Weiss, X. D. Duan, H. C. Cheng, Y. Huang, X. F. Duan, Nat. Rev. Mater. 2016, 1, 16042; c) F. Liu, W. J. Wu, Y. S. Bai, S. H. Chae, Q. Y. Li, J. Wang, J. Hone, X. Y. Zhu, Science 2020, 367, 903-906.
- [3] a) A. J. Mannix, B. Kiraly, M. C. Hersam, N. P. Guisinger, Nat. Rev. Chem. 2017, 1, 0014; b) G. Li, Y. Y. Zhang, H. Guo, L. Huang, H. L. Lu, X. Lin, Y. L. Wang, S. X. Du, H. J. Gao, Chem. Soc. Rev. 2018, 47, 6073-6100; c) L. F. Li, Y. L. Wang, S. Y. Xie, X. B. Li, Y. Q. Wang, R. T.

- Wu, H. B. Sun, S. B. Zhang, H. J. Gao, *Nano Lett.* **2013**, *13*, 4671-4674; d) L. F. Li, S. Z. Lu, J. B. Pan, Z. H. Qin, Y. Q. Wang, Y. L. Wang, G. Y. Cao, S. X. Du, H. J. Gao, *Adv. Mater.* **2014**, *26*, 4820-4824; e) Y. L. Wang, L. F. Li, W. Yao, S. R. Song, J. T. Sun, J. B. Pan, X. Ren, C. Li, E. Okunishi, Y. Q. Wang, E. Y. Wang, Y. Shao, Y. Y. Zhang, H. T. Yang, E. F. Schwier, H. Iwasawa, K. Shimada, M. Taniguchi, Z. H. Cheng, S. Y. Zhou, S. X. Du, S. J. Pennycook, S. T. Pantelides, H. J. Gao, *Nano Lett.* **2015**, *15*, 4013-4018.
- [4] a) A. J. Mannix, X. F. Zhou, B. Kiraly, J. D. Wood, D. Alducin, B. D. Myers, X. L. Liu, B. L. Fisher, U. Santiago, J. R. Guest, M. J. Yacaman, A. Ponce, A. R. Oganov, M. C. Hersam, N. P. Guisinger, Science 2015, 350, 1513-1516; b) B. J. Feng, J. Zhang, Q. Zhong, W. B. Li, S. Li, H. Li, P. Cheng, S. Meng, L. Chen, K. H. Wu, Nat. Chem. 2016, 8, 564-569.
- [5] X. L. Liu, Q. C. Li, Q. Y. Ruan, M. S. Rahn, B. I. Yakobson, M. C. Hersam, *Nat. Mater.* 2022, 21, 35-40.
- [6] N. Gao, X. Wu, X. Jiang, Y. Z. Bai, J. J. Zhao, Flatchem 2018, 7, 48-54.
- Y. W. Mu, B. T. Wang, S. D. Li, F. Ding, Nanoscale 2022, 14, 9754-9761.
- [8] X. F. Zhou, A. R. Oganov, Z. H. Wang, I. A. Popov, A. I. Boldyrev, H. T. Wang, *Phys. Rev. B* 2016, 93, 085406.
- [9] F. X. Ma, Y. L. Jiao, G. P. Gao, Y. T. Gu, A. Bilic, Z. F. Chen, A. J. Du, Nano Lett. 2016, 16, 3022-3028.
- [10] S. G. Xu, B. B. Zheng, H. Xu, X. B. Yang, J. Phys. Chem. C 2019, 123, 4977-4983.
- [11] C. Y. Chen, H. F. Lv, P. Zhang, Z. W. Zhuo, Y. Wang, C. Ma, W. B. Li, X. G. Wang, B. J. Feng, P. Cheng, X. J. Wu, K. H. Wu, L. Chen, *Nat. Chem.* 2022, 14, 25-31.
 - a) E. A. Pozzi, G. Goubert, N. Chiang, N. Jiang, C. T. Chapman, M. O. McAnally, A.-I. Henry, T. Seideman, G. C. Schatz, M. C. Hersam, R. P. V. Duyne, Chem Rev 2017, 117, 4961-4982; b) J. F. Schultz, Nat. Rev. Phys. 2022, https://doi.org/10.1038/s42254-42022-00537-42250; c) R. Zhang, Y. Zhang, Z. C. Dong, S. Jiang, C. Zhang, L. G. Chen, L. Zhang, Y. Liao, J. Aizpurua, Y. Luo, J. L. Yang, J. G. Hou, Nature 2013, 498, 82-86; d) J. Lee, K. T. Crampton, N. Tallarida, V. A. Apkarian, Nature 2019, 568, 78-82; e) J. Y. Xu, X. Zhu, S. J. Tan, Y. Zhang, B. Li, Y. Z. Tian, H. Shan, X. F. Cui, A. D. Zhao, Z. C. Dong, J. L. Yang, Y. Luo, B. Wang, J. G. Hou, Science 2021, 371, 818-822; f) J. H. Zhong, X. Jin, L. Y. Meng, X. Wang, H. S. Su, Z. L. Yang, C. T. Williams, B. Ren, Nat Nanotechnol 2017, 12, 132-136; g) R. B. Jaculbia, H. Imada, K. Miwa, T. Iwasa, M. Takenaka, B. Yang, E. Kazuma, N. Hayazawa, T. Taketsugu, Y. Kim. Nat Nanotechnol 2020, 15, 105-110; h) H. Yin, L.-Q. Zheng, W. Fang, Y.-H. Lai, N. Porenta, G. Goubert, H. Zhang, H.-S. Su, B. Ren, J. O. Richardson, J.-F. Li, R. Zenobi, Nat Catal 2020, 3, 834-842; i) N. Jiang, N. H. Chiang, L. R. Madison, E. A. Pozzi, M. R. Wasielewski, T. Seideman, M. A. Ratner, M. C. Hersam, G. C. Schatz, R. P. Van Duyne, Nano Lett. 2016, 16, 3898-3904; j) S. Mahapatra, Y. Y. Ning, J. F. Schultz, L. F. Li, J. L. Zhang, N. Jiang, Nano Lett. 2019, 19, 3267-3272; k) J. F. Schultz, L. Li, S. Mahapatra, C. Shaw, X. Zhang, N. Jiang, J. Phys. Chem. C 2020, 124, 2420-2426.
- [13] a) S. Mahapatra, L. Li, J. F. Schultz, N. Jiang, J. Chem. Phys. 2020, 153, 010902; b) J. F. Schultz, S. Mahapatra, L. F. Li, N. Jiang, Appl. Spectrosc. 2020, 74, 1313-1340.
- [14] a) L. F. Li, J. F. Schultz, S. Mahapatra, Z. Y. Lu, X. Zhang, N. Jiang, Nat. Commun. 2022, 13, 1796; b) L. F. Li, J. F. Schultz, S. Mahapatra, X. L. Liu, C. Shaw, X. Zhang, M. C. Hersam, N. Jiang, J. Am. Chem. Soc. 2021, 143, 15624-15634.
- [15] X. L. Liu, L. Q. Wang, S. W. Li, M. S. Rahn, B. I. Yakobson, M. C. Hersam, Nat. Commun. 2019, 10, 1642.
- [16] X. L. Liu, M. S. Rahn, Q. Y. Ruan, B. I. Yakobson, M. C. Hersam, Nanotechnology 2022, 33, 235702.
- [17] a) W. W. Luo, G. Liu, Z. H. Xu, Z. Y. Zhou, X. Wang, C. Y. Ouyang, S. Q. Liu, Comp Mater Sci 2017, 140, 261-266; b) Y. W. Mu, S. D. Li, J. Phys. Chem. C 2020, 124, 28145-28151.
- [18] Y. F. Dai, S. Ni, Z. Y. Li, J. L. Yang, J. Phys.: Condens. Matter 2013, 25, 405301.
- [19] a) Z. H. Zhang, J. Yin, X. F. Liu, J. D. Li, J. H. Zhang, W. L. Guo, J. Phys. Chem. Lett. 2016, 7, 867-873; b) A. M. Suarez, L. R. Radovic, E. Bar-Ziv, J. O. Sofo, Phys. Rev. Lett. 2011, 106, 146802.

[20] Q. C. Li, V. S. C. Kolluru, M. S. Rahn, E. Schwenker, S. W. Li, R. G. Hennig, P. Darancet, M. K. Y. Chan, M. C. Hersam, *Science* 2021, 371, 1143-1148.



Entry for the Table of Contents



Scanning tunneling microscopy-based tip-enhanced Raman spectroscopy (TERS) was used to study the local chemical properties of bilayer synthetic two-dimensional boron (i.e., borophene) with atomic-scale spatial resolution. TERS established the chemical fingerprint of bilayer borophene that is correlated with the vibration of interlayer boron-boron bonds and demonstrated the chemical stability of bilayer borophene with single-bond (B–O) sensitivity by exposure to controlled oxidizing conditions in ultrahigh vacuum.

